Earth and Planetary Science Letters 369–370 (2013) 86–97

Contents lists available at SciVerse ScienceDirect

Earth and Planetary Science Letters

journal homepage: www.elsevier.com/locate/epsl

A new perspective on boundary scavenging in the North Pacific Ocean

Christopher T. Hayes [a,b,*], Robert F. Anderson [a,b], Samuel L. Jaccard [c], Roger François [d], Martin Q. Fleisher [a], Maureen Soon [d], Rainer Gersonde [e]

[a] Lamont-Doherty Earth Observatory of Columbia University, Palisades, NY, USA
[b] Department of Earth and Environmental Sciences, Columbia University, New York, NY, USA
[c] Geological Institute, Department of Earth Sciences, ETH Zürich, Switzerland
[d] Department of Earth and Ocean Sciences, University of British Columbia, Vancouver, BC, Canada
[e] Alfred Wegener Institute for Polar and Marine Research, Bremerhaven, Germany

ARTICLE INFO

Article history:
Received 6 August 2012
Received in revised form
12 February 2013
Accepted 8 March 2013
Editor: G. Henderson
Available online 19 April 2013

Keywords:
thorium
protactinium
scavenging
North Pacific Ocean
INOPEX
line P

ABSTRACT

Boundary scavenging, or the enhanced removal of adsorption-prone elements from the ocean in areas of high particle flux, is an often cited, though not well-quantified, concept used to understand the oceanic distribution of many trace metals. Because ^{230}Th and ^{231}Pa are produced uniformly from uranium decay and removed differentially by scavenging, the process of boundary scavenging can be elucidated by a more detailed knowledge of their water column distributions. To this end, filtered seawater was collected across the gradients in particle flux which span the subarctic Pacific: in the west during the Innovative North Pacific Experiment (INOPEX) and in the east along Line P. Lateral concentration gradients of dissolved ^{230}Th are small throughout the subarctic Pacific at 12 sites of variable particle flux. This contradicts the prediction of the traditional boundary scavenging model. A compilation of water column data from throughout the North Pacific reveals much larger lateral concentration gradients for ^{230}Th between the subarctic North Pacific and subtropical gyre, over lateral gradients in scavenging intensity similar to those found within the subarctic. This reflects a biogeochemical-province aspect to scavenging. Upper water column distributions of ^{231}Pa and ^{231}Pa/^{230}Th ratio are consistent with the influence of scavenging by biogenic opal, while deep waters (>2.5 km) reveal an additional ^{231}Pa sink possibly related to manganese oxides produced at continental margins or ridge crests.

1. Introduction

Boundary scavenging (Bacon et al., 1976; Spencer et al., 1981) is a classic mechanism used to understand the cycling of chemical elements having the tendency to adsorb onto sinking particles, or to be scavenged. Scavenging (Goldberg, 1954) affects the cycling of many trace elements from micronutrients, such as Fe (Boyd and Ellwood, 2010) or Co (Bown et al., 2011), to tracers of dust deposition, such as Al (Measures and Vink, 2000) or Th (Hsieh et al., 2011). It is therefore valuable to better understand the nature of the boundary scavenging process.

The boundary scavenging mechanism predicts that those elements whose residence times are long enough to allow basin-wide isopycnal diffusion (>100 yr), such as Pa, will be transported away from areas of low scavenging intensity to be removed in areas of high scavenging intensity (often associated with ocean boundaries) (Bacon, 1988). This lateral transfer reduces the concentration difference between ocean margin and ocean interior imposed by differential scavenging intensities. An element like Th, on the other hand, whose residence time (<50 yr) is short enough to limit isopycnal transport, should therefore display concentrations which scale inversely with scavenging intensity. More detailed accounts of the development of boundary scavenging are given elsewhere (Anderson et al., 1990; François, 2007; Roy-Barman, 2009; Rutgers v. d. Loeff and Geibert, 2008), but few historical data exist to elucidate it in the dissolved phase of the water column. The prime objectives of this study are to relay new measurements of dissolved ^{230}Th and ^{231}Pa throughout the North Pacific and offer a new perspective on the traditional boundary scavenging concept.

The North Pacific Ocean lacks active deep water formation, which is known to influence ^{231}Pa/^{230}Th distributions in the Atlantic where surface waters of low radionuclide concentration are injected to depth (Luo et al., 2010; Moran et al., 2002). We cannot, however, discount quantitatively the influence of the Pacific Meridional Overturning Circulation (PMOC) on dissolved ^{231}Pa/^{230}Th in the North Pacific, namely the northward inflow of Lower Circumpolar Deep Water (LCDW) and upwelling to form southward flowing North Pacific Deep Water (NPDW). We defer to

* Correspondence to: Comer 427, 61 Route 9W, Palisades, NY 10964, USA. Tel.: +1 845 365 8572; fax: +1 845 365 8155.
E-mail address: cth@ldeo.columbia.edu (C.T. Hayes).

0012-821X/$ - see front matter © 2013 Elsevier B.V. All rights reserved.
http://dx.doi.org/10.1016/j.epsl.2013.03.008

modeling studies for a more complete treatment of PMOC (Luo et al., 2012) but signify in our work where the influence of overturning may be important. Aside from overturning, we expect ^{231}Pa and ^{230}Th distributions to be determined by the balance between production due to U decay, removal by scavenging, and redistribution by mixing. Below we elaborate on how we approach each of these terms.

The uniform distribution of ^{235}U and ^{234}U (Andersen et al., 2010; Delanghe et al., 2002; Robinson et al., 2004; Weyer et al., 2008) amounts to a constant and uniform production for ^{231}Pa and ^{230}Th, respectively, throughout the ocean. The production term, P, depends on the seawater concentration of U, which as a conservative element, varies with salinity (Chen et al., 1986).

Our basis for understanding scavenging is the one-dimensional reversible-scavenging model (Bacon and Anderson, 1982). Neglecting lateral inputs, this model predicts a linear increase with depth (z) for the concentration of dissolved (C_d) and particulate (C_p) phases for *in-situ*-produced scavenged elements. Given a group of small particles, which assumedly carry most of the scavenged element and sink at a constant speed, S, the concentrations are

$$C_d \cong \frac{Pz}{SK} \tag{1}$$

$$C_p = \frac{Pz}{S} \tag{2}$$

C_d and C_p are expressed in units per volume of seawater. K is the distribution coefficient between particulate and dissolved phases (c_p/c_d), which may vary as a function of particle concentration or particle composition. If lateral effects can be neglected, distributions of C_d, the primary subject of study here, are expected to respond inversely to scavenging intensity, parameterized by SK.

When spatial concentration gradients exist, mixing by eddy diffusion will transport radionuclides from areas of high concentration to areas of low concentration. However, for the case of scavenged elements, one must consider the timescale (Δt) required for mixing to take place over a certain length scale (Δx) against the residence time (τ) of the element or isotope in question. Spatial concentration gradients will be undisturbed if $\Delta t \gg \tau$. On the other hand, imposed gradients could be mixed away if $\Delta t \ll \tau$. In one-dimension, as presented by Roy-Barman (2009), the root-mean-square displacement ($\sqrt{(\Delta x)^2}$, given here for simplicity as Δx) of a randomly walking water parcel is

$$\Delta x = \sqrt{2K_{mix}\Delta t} \tag{3}$$

where K_{mix} is the coefficient of eddy diffusion. Following Okubo et al. (2012), when substituting Δt by τ, Δx then represents the maximum length scale over which mixing influences spatial concentration gradients. Typical values in the North Pacific of isopycnal (lateral), K_H, and diapycnal (vertical), K_ρ, eddy diffusivity are 10^3 m^2 s^{-1} and 10^{-4} m^2 s^{-1}, respectively (Kawabe, 2008).

The mixing length-scale argument calls for an appropriate definition of τ. Assuming steady-state, neglecting advective or diffusive inputs, the residence time of dissolved ^{230}Th (^{231}Pa) at any point is given by its concentration divided by the sum of its *in situ* sources: production via uranium decay and desorption, the latter of which unfortunately cannot be characterized with measurements of only C_d. Alternatively, the inventory of C_d from the surface to some depth divided by the depth-integrated P results in the average time a dissolved nuclide resides in the integrated water column before being removed to deeper water by scavenging, irrespective of desorption within that depth zone. We find this integrated residence time to be most appropriate when considering the influence of mixing on dissolved nuclide distributions in the absence of constraints on desorption. Nonetheless, this residence time is not independent of advective or diffusive inputs where they exist. The integrated residence time will be an overestimate at locations which receive ^{230}Th (^{231}Pa) by circulation and an underestimate at locations where ^{230}Th (^{231}Pa) is removed by circulation.

2. Materials and methods

2.1. Dissolved Th (Pa) sampling and analysis

The new data presented here were produced by groups at the Lamont-Doherty Earth Observatory (L-DEO) and the University of British Columbia (UBC). Seven profiles of dissolved ^{230}Th, ^{231}Pa, and ^{232}Th from the SO202-INOPEX cruise of July–August 2009 (Gersonde, 2012) (SO202-stations in Fig. 1) were produced at L-DEO. Five profiles of dissolved ^{230}Th from the eastern subarctic Pacific collected in summer 2006 (P and Z stations in Fig. 1, referred to collectively as Line P in the text) were produced at UBC.

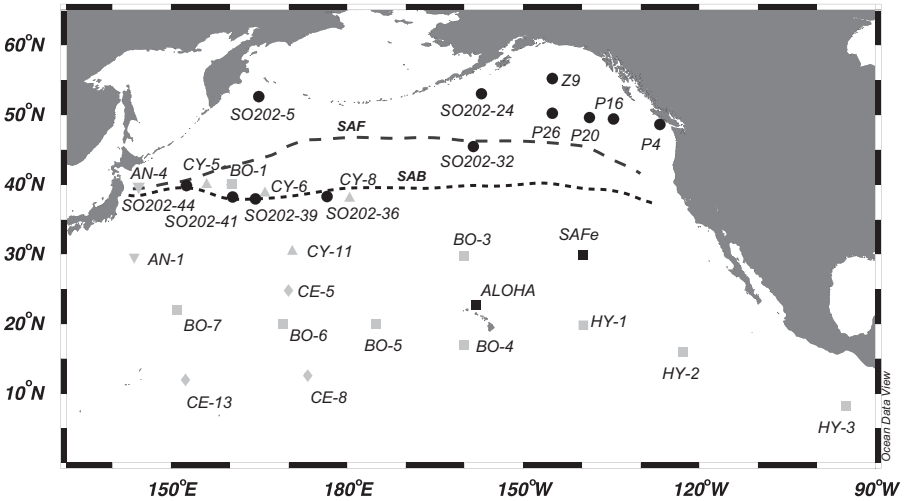

Fig. 1. Map of station locations for dissolved radionuclide data presented in the paper (black circles and squares) and those for which total radionuclide data has been reported: gray triangles (Nozaki et al., 1981), gray diamonds (Nozaki and Nakanishi, 1985), gray inverted triangles (Nozaki et al., 1998), and gray squares (Okubo et al., 2012). Dashed and dotted lines approximate the subarctic front (SAF) and subarctic boundary (SAB), respectively, as drawn by Harrison et al. (2004). SO202- refers to the INOPEX cruise; P and Z stations refer to the Line P cruise (see Section 2.1).

Additionally we draw from reported profiles of dissolved ^{230}Th and ^{231}Pa from the Hawaii Ocean Time-series collected in 2002 (ALOHA station in Fig. 1) produced by the UBC group (François, 2007) and the 2009 "baseline" profile of dissolved ^{230}Th, ^{231}Pa, and ^{232}Th from the US GEOTRACES Intercalibration (SAFe station in Fig. 1) produced at L-DEO (Anderson et al., 2012). Hydrographic data for the newly reported sample locations are included in the Supplementary Material. INOPEX data are available through PANGAEA (pangaea.de) and the BCO-DMO data repository (bcodmo.org). SAFe data are available at BCO-DMO.

Both the INOPEX and Line P cruises used similar methods for sampling dissolved (<0.45 μm) radionuclides. The INOPEX cruise is considered GEOTRACES compliant (see geotraces.org). Detailed sampling procedures are described by Anderson et al. (2012). Logistics for both cruises did not permit the collection of sufficient particulate material for radionuclide analysis.

Radionuclide concentrations were determined by isotope dilution Inductively Coupled Plasma Mass Spectrometry at L-DEO (^{230}Th, ^{232}Th, and ^{231}Pa) and UBC (^{230}Th). Th and Pa were preconcentrated along with ^{229}Th and ^{233}Pa by co-precipitation with 15–50 mg of added Fe. After HNO_3–$HClO_4$–HF digestion of the precipitate, Th and Pa were isolated and purified using anion exchange chromatography (Bio-rad resin AG1-X8). Full details on L-DEO procedures are reported by Anderson et al. (2012) and UBC procedures are reported by Choi et al. (2001).

For samples stored for more than a few months prior to Th/Pa purification, a small correction must be made for the ingrowth of ^{230}Th or ^{231}Pa by uranium decay during the time period between sample collection and U–Th/Pa separation (~0.03 dpm m^{-3} ^{230}Th and 0.002 dpm m^{-3} ^{231}Pa are ingrown annually). U concentrations in the samples were estimated using the bottle salinity measured from the CTD. For a full description of this correction, see the metadata associated with the INOPEX data at BCO-DMO.

A correction was also made for the ^{230}Th and ^{231}Pa added to the dissolved pool through the partial dissolution of lithogenic minerals, assuming an average lithogenic U/Th ratio, secular equilibrium within the lithogenic material and congruent dissolution, based on measured dissolved ^{232}Th. We used ^{230}Th/^{232}Th$=4.0\times10^{-6}$ mol/mol (Roy-Barman et al., 2009) and ^{231}Pa/^{232}Th$=8.8\times10^{-8}$ mol/mol (Taylor and McLennan, 1985) as representative of detrital Th and Pa, respectively. This correction was possible for the INOPEX and SAFe data but not for the Line P or ALOHA data, where ^{232}Th was not measured. Detrital ^{230}Th was found to be a significant fraction ($>10\%$) of the dissolved ^{230}Th only in surface waters (<200 m) proximal to mineral dust sources. Detrital ^{231}Pa was 1% of the dissolved ^{231}Pa in the INOPEX samples at its highest and $<0.5\%$ below 200 m. Dissolved ^{230}Th from ALOHA is likely less than 1% detrital below surface waters based on historical ^{232}Th measurements there (Roy-Barman et al., 1996) and detrital ^{231}Pa even less. The Line P stations are outside of the influence of Asian dust deposition, but detrital ^{230}Th advected from margin sediments is possible.

2.2. Use of total ^{230}Th and ^{231}Pa data

We draw upon previously reported profiles of total (dissolved+particulate) ^{230}Th (Nozaki et al., 1981, 1987; Nozaki and Nakanishi, 1985; Okubo et al., 2012) and total ^{231}Pa (Nozaki and Nakanishi, 1985; Nozaki et al., 1998) (see Fig. 1). We converted total ^{230}Th (^{231}Pa) to dissolved ^{230}Th (^{231}Pa), as an attempt to remove the influence of particulate ^{230}Th (^{231}Pa), using the equation dissolved=total$*(1-K)$. We used average values from the most geographically relevant measurements of K, from ALOHA, $K=0.18\pm0.09$ for ^{230}Th (Roy-Barman et al., 1996), and from AN-1, $K=0.04\pm0.01$ for ^{231}Pa (Nozaki et al., 1998). The uncertainty in K was propagated in our dissolved estimates, but K at a specific location may be outside the cited ranges. Total radionuclides are not corrected for detrital contributions. All radionuclide concentrations have been converted into volumetric radioactivity units (dpm m^{-3}), assuming constant seawater density (1026 kg m^{-3}).

2.3. Hydrographic considerations

We use the term subarctic somewhat loosely to distinguish the INOPEX and Line P stations from the (sub)tropical sites in Fig. 1. While stations SO202-36, -39, -41, and -44 are a few degrees south of the Subarctic Front defined by the 4 °C isotherm at 100 m depth, they are nearly on the Subarctic Boundary defined by the surface salinity front of $S=34$ (Yasuda, 2003). The Subarctic Boundary roughly corresponds to the southern and northern limits, respectively, of the cyclonic subarctic gyre and the anticyclonic subtropical gyre which are the major expressions of surface circulation in the North Pacific. There is also a relatively weak shallow overturning cell with a net northward transport of subtropical water balanced by a southward interior flow, in the form of North Pacific Intermediate Water (NPIW) (Macdonald et al., 2009).

In terms of deep circulation, Kawabe and Fujio (2010) have mapped observed flows of LCDW entering the western North Pacific at approximately 4.5 km depth, which travel north and east throughout the basin. LCDW along with the overlaying Upper Circumpolar Deep Water (UCDW) eventually upwell at various locations to become southward flowing NPDW across the basin between ~1.5–3 km depth (Macdonald et al., 2009). This represents the schematic pattern of deep overturning in the North Pacific, but advective features may not be the dominant circulation of the basin. Circuitous, random-walk circulation generated by eddies in the deep North Pacific apparently dominate inter-basin water flux pathways (Holzer and Primeau, 2006, 2008). In the ensuing analysis, we refrain from adhering to an "advective-ocean" circulation framework and consider the influence of eddy diffusion more generally.

2.4. Indicators of expected scavenging intensity

Satellite-derived estimates of net primary productivity (NPP) are not directly related to scavenging intensity, but more biological productivity at the surface likely results in a greater sinking flux of scavenging particles. In lieu of detailed observations of the particulate matter and its scavenging characteristics at our study sites (surface area, chemical composition, aggregation tendency, etc.) and due to the long-term nature and excellent geographical coverage of satellite records, we appeal to NPP as a qualitative indicator for spatial variability in scavenging intensity. Monthly SeaWiFS-NPP data (1997–2009, 1/6°-resolution) were time-weighted averaged, ignoring missing values (Fig. S1) (http://www.science.oregonstate.edu/ocean.productivity) (Behrenfeld and Falkowski, 1997).

Export production (EP), an alternative qualitative indicator of scavenging intensity (Coale and Bruland, 1987), is defined as the sinking flux of particulate organic carbon from the euphotic zone to the ocean interior (Eppley and Peterson, 1979). The ratio of EP to NPP is termed the ef-ratio and can be estimated as a function of sea surface temperature (SST) and NPP itself (Laws et al., 2000). Export production estimates were derived by calculating the ef-ratio (Laws et al., 2000) and multiplying by the aforementioned long-term average NPP. SSTs for the ef-ratio algorithm were from the World Ocean Atlas 2009 (Locarnini et al., 2010). One reason that EP may more accurately reflect variations in scavenging intensity than does NPP is that higher EP can be associated with a greater flux of ballasting minerals (biogenic opal, $CaCO_3$, and aluminosilicates) (Boyd and Trull, 2007; Bradtmiller et al., 2010; Honda and Watanabe, 2010) which also contribute to scavenging.

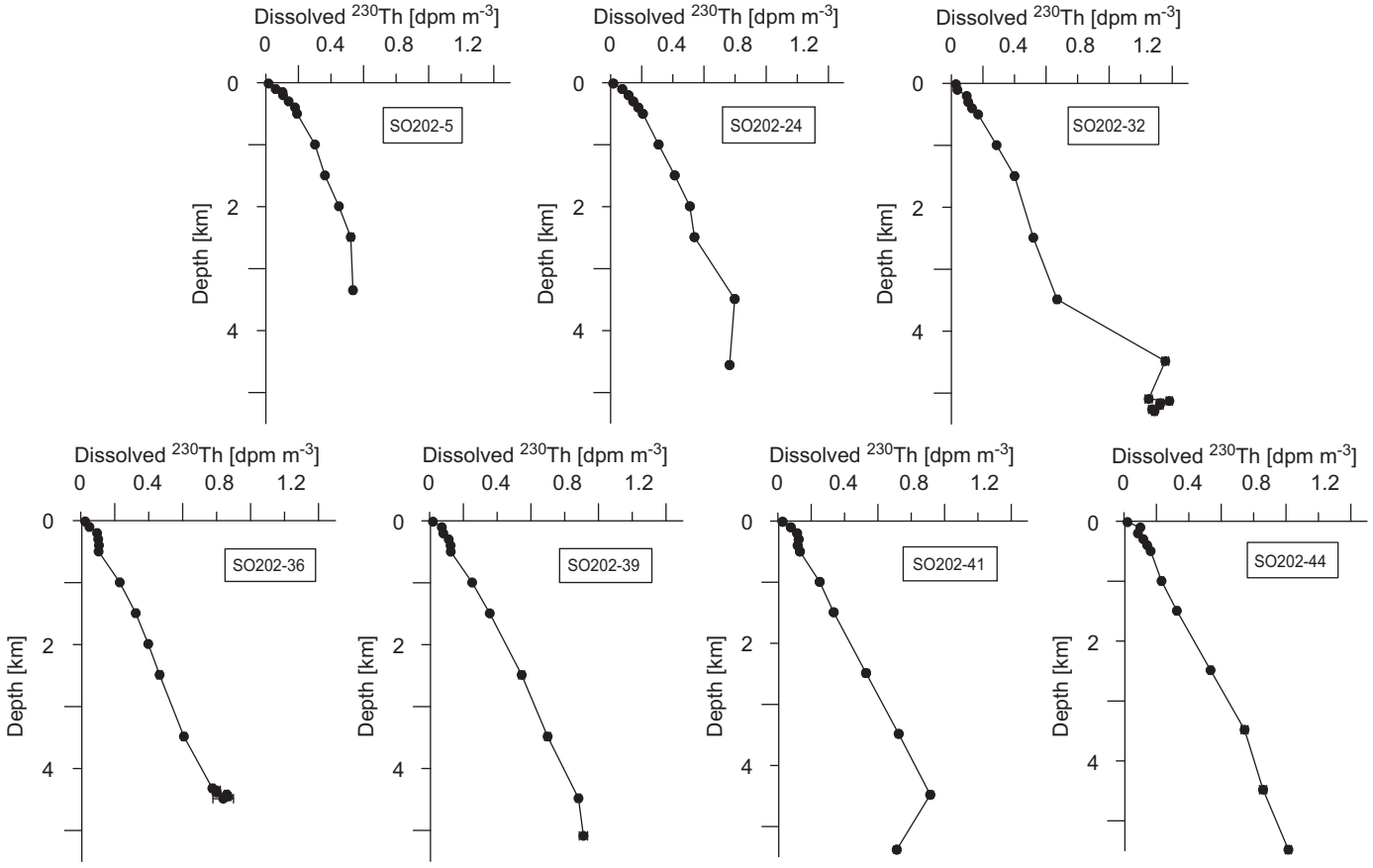

Fig. 2. Depth profiles of dissolved ^{230}Th from the INOPEX locations (SO202- in Fig. 1). These data have been corrected for the detrital ^{230}Th based on measured dissolved ^{232}Th (see Section 2.2). The deepest sample in each profile is 5–15 m above the seafloor. Where error bars are not visible they are smaller than the symbol size.

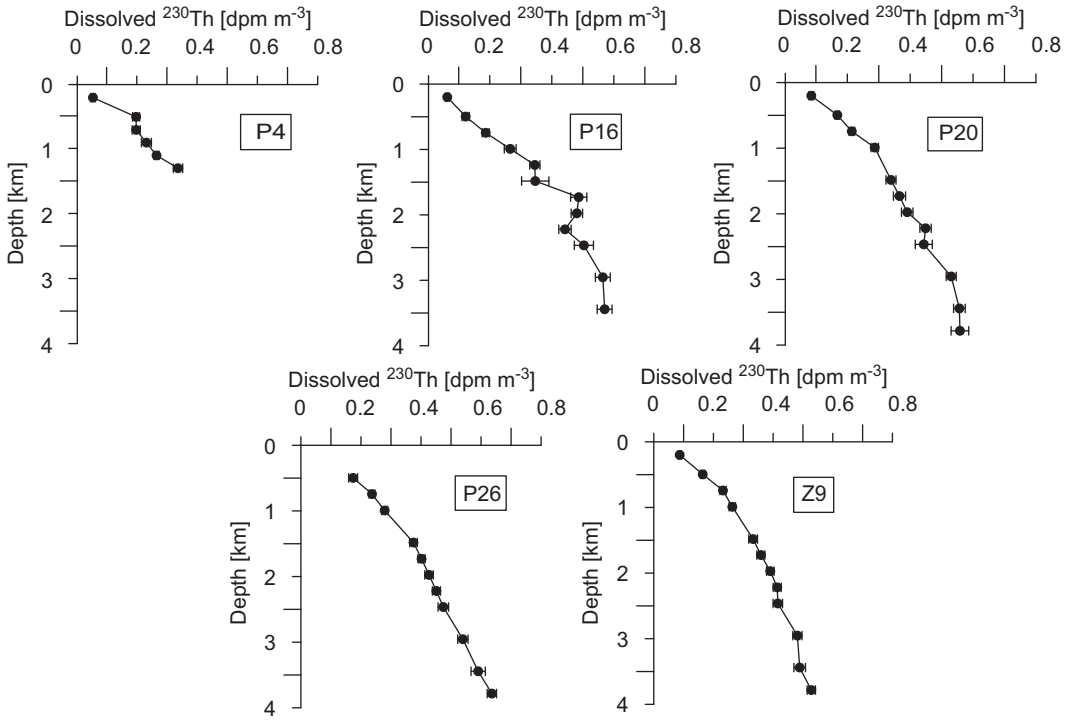

Fig. 3. Depth profiles of dissolved ^{230}Th from Line P (P and Z stations in Fig. 1). These data have not been corrected for detrital ^{230}Th (see Section 2.2). The deepest sample in each profile is between 38 and 537 m above the seafloor (see Table 1). Where error bars are not visible they are smaller than the symbol size.

Table 1
Sea surface temperature (SST), Net Primary Productivity (NPP), ef-ratio, Export Productivity (EP) and dissolved inventories of ^{230}Th and ^{231}Pa in the upper 2.5 km of the water column for station locations used in this study; see Fig. S1 in the Supplementary material for a high resolution map of NPP in relation to station locations.

Station	Latitude (°N)	Longitude (°E)	Water depth (m)	SST (°C)	NPP g C m^{-2} yr^{-1}	ef-ratio	EP g C m^{-2} yr^{-1}	Diss. ^{230}Th inventory (2.5 km) dpm m^{-2}	± dpm m^{-2}	Diss. ^{2310}Pa inventory (2.5 km) dpm m^{-2}	± dpm m^{-2}	Reference
BO-1	40	160	5588	12.9	212	0.55	116	1218	60			Okubo et al. (2012) (Based on total ^{230}Th)
BO-3	30	−160	5774	21.6	108	0.27	30	1888	87			Okubo et al. (2012) (Based on total ^{230}Th)
BO-4	17	−160	5591	25.8	80	0.20	16	1598	72			Okubo et al. (2012) (Based on total ^{230}Th)
BO-5	20	−175	5307	26.2	63	0.20	13	1769	82			Okubo et al. (2012) (Based on total ^{230}Th)
BO-6	20	169	5372	26.9	53	0.20	10	1658	76			Okubo et al. (2012) (Based on total ^{230}Th)
BO-7	22	151	5623	26.9	56	0.20	11	1632	74			Okubo et al. (2012) (Based on total ^{230}Th)
HY-1	20	−140	5287	23.4	96	0.24	23	1071	46			Okubo et al. (2012) (Based on total ^{230}Th)
HY-2	16	−123	4229	25.1	115	0.21	24	1077	45			Okubo et al. (2012) (Based on total ^{230}Th)
HY-3	8	−95	3656	27.6	201	0.18	35	607	27			Okubo et al. (2012) (Based on total ^{230}Th)
CY-5	40.017	156.033	5523	13.3	220	0.53	117	1123	78			Nozaki et al. (1981) (Based on total ^{230}Th)
CY-6	39.017	166	5576	14.7	205	0.47	97	668	50			Nozaki et al. (1981) (Based on total ^{230}Th)
CY-8	38.05	180.267	5553	15.7	190	0.44	83	575	58			Nozaki et al. (1981) (Based on total ^{230}Th)
CY-11	30.533	170.65	5523	22.2	147	0.26	39	933	55			Nozaki et al. (1981) (Based on total ^{230}Th)
CE-5	25	169.983	5960	25.4	67	0.21	14	1030	84			Nozaki and Nakanishi (1985) (Based on total ^{230}Th and ^{231}Pa)
CE-8	12.75	173.233	5686	27.7	47	0.19	9	1242	70	1095	60	Nozaki and Nakanishi (1985) (Based on total ^{230}Th and ^{231}Pa)
CE-13	12	152.5	5883	28.3	40	0.19	8	1331	89	817	51	Nozaki and Nakanishi (1985) (Based on total ^{230}Th and ^{231}Pa)
AN-1	29.7	143.8	9750	23.2	145	0.24	35	872	63	897	68	Nozaki et al. (1998) (Based on total ^{230}Th and ^{231}Pa)
AN-4	39.6	144.4	7585	13.7	300	0.52	155	644	51			Nozaki et al. (1998) (Based on total ^{230}Th and ^{231}Pa)
IN-5	52.696	164.919	3364	5.0	167	0.68	113	795	7	226	11	Present work
IN-24	53.002	−157.193	4567	6.8	216	0.68	146	865	7	245	8	Present work
IN-32	45.5	−158.5	5301	9.5	162	0.67	108	794	9	272	12	Present work
IN-36	38.19	176.696	4524	15.9	194	0.43	84	662	8	321	13	Present work
IN-39	38.011	164.445	5098	15.9	217	0.43	94	745	10	332	20	Present work
IN-1	38.413	160.335	5392	15.9	216	0.43	93	728	13	312	16	Present work
IN-44	39.801	152.351	5505	14.9	242	0.46	112	725	11	294	12	Present work
ALOHA	22.75	−158	4800	24.8	101	0.21	21	1313	6	922	12	François (2007)
SAFE	30	−140	4750	20.2	111	0.30	34	1494	20	756	16	Anderson et al. (2012)
P16	49.283	−134.667	3550	10.4	167	0.65	108	739	12			Present work
P20	49.567	−138.667	4020	9.7	156	0.66	103	701	9			Present work
P26	50	−145	4320	8.3	165	0.67	111	737	8			Present work
Z9	55	−145	4025	7.6	183	0.67	123	680	7			Present work
P4	48.633	−126.65	1323	11.3	436	0.62	268					Present work

3. Results and discussion

3.1. Distribution of ^{230}Th in the subarctic Pacific

3.1.1. Uniformity of INOPEX and Line P ^{230}Th profiles

The depth profiles of dissolved ^{230}Th from the INOPEX (Fig. 2) and Line P (Fig. 3) locations are all nearly linear and quite similar to each other. Linear profiles are consistent with reversible scavenging (which neglects lateral transport) (Bacon and Anderson, 1982). We note, however, that relatively linear ^{230}Th profiles are not inconsistent with some lateral ^{230}Th transport (discussed further below) (Roy-Barman, 2009; Venchiarutti et al., 2008).

The ^{230}Th data fall within the linear depth profiles described by $[^{230}\text{Th}] = (0.05 \pm 0.05)\ \text{dpm m}^{-3} + (0.2 \pm 0.05)\ \text{dpm m}^{-3}\ \text{km}^{-1} * z$, except at SO202-32 below 4.4 km. In other words, ^{230}Th concentrations at a given depth vary spatially by no more than about 25%. Our indicators for scavenging intensity, on the other hand, range from 156 to 436 g C m^{-2} yr^{-1} (a factor of 2.8) in NPP and 84 to 268 g C m^{-2} yr^{-1} (a factor of 3.2) in EP among the stations (see Table 1). A section across the North Pacific (Fig. 4) displays the uniformity of [^{230}Th] on a given isopycnal throughout the bulk of the water column. Positive (SO202-32) and negative (SO202-39, SO202-41) concentration anomalies near the seafloor are exceptions to this uniformity (Section 3.1.2).

The spatial homogeneity of ^{230}Th is surprising in light of the strong gradients in expected scavenging intensity in this region, especially near the continental margins. The INOPEX stations near 40°N (SO202-36, -39, -41, and -44) are situated on an east–west NPP and EP gradient of 23 and 13 mg C m^{-2} yr^{-1} km^{-1}, respectively. Gradients are calculated by the difference in NPP (EP) over the distance between stations (SO202-36–SO202-44 in this case). The ^{230}Th profiles from these 4 stations are consistent within error with the margin profile of dissolved ^{230}Th (converted from total) at station AN-4 (Nozaki et al., 1998), revealing little lateral gradients over even a larger transect and gradient in scavenging intensity (lateral NPP and EP gradients of 38 and 25 mg C m^{-2} yr^{-1} km^{-1}, respectively). The true gradient in scavenging intensity is most likely greater than that based solely on NPP or EP because we also expect a positive east–west gradient in the flux of aerosol dust (Mahowald et al., 2005) and biogenic opal (Honjo et al., 2008; Shibamoto and Harada, 2010) on the western margin. On the eastern margin (Line P), we estimate even larger lateral gradients in scavenging intensity (NPP and EP gradients of 203 and 118 mg C m^{-2} yr^{-1} km^{-1}, respectively).

Lateral concentration gradients imposed by variable scavenging intensity could be overcome by horizontal homogenization by mixing along isopycnals, and this must be addressed in light of the observed lack of lateral gradient in [^{230}Th] in the subarctic. Using station SO202-44 as representative of the region, the integrated residence time of dissolved ^{230}Th is 11 yr in the upper 2.5 km and is 22 yr in the full water column (5.5 km). Using Eq. 3 ($K_H = 10^3$ m^2 s^{-1}), a timescale of 11 and 22 yr allows diffusion to propagate to a radius of about 830 km and 1200 km, respectively. The east–west transects IN36-44 and Line P are 2100 km and 1300 km in distance, respectively. Therefore, lateral mixing does not influence ^{230}Th distributions in the upper 2.5 km of the water column. However, we cannot rule out some ^{230}Th redistribution back across lateral gradients in scavenging intensity in the deepest depths of the subarctic Pacific, as the deep mixing lengths are comparable to the section distances. If, however, SO202-44 were receiving a small input of ^{230}Th by lateral mixing, as might be expected at the "high-scavenging"-end of the 40°N transect, the cited residence times would be an overestimate and the corresponding mixing lengths would be smaller. Advection across concentration gradients will also contribute to a redistribution of ^{230}Th (Roy-Barman, 2009), and strong deep boundary currents have been observed in the Northwest Pacific (Owens and Warren, 2001). However, given that these currents are generally non-continuous and often change direction we cannot quantify the

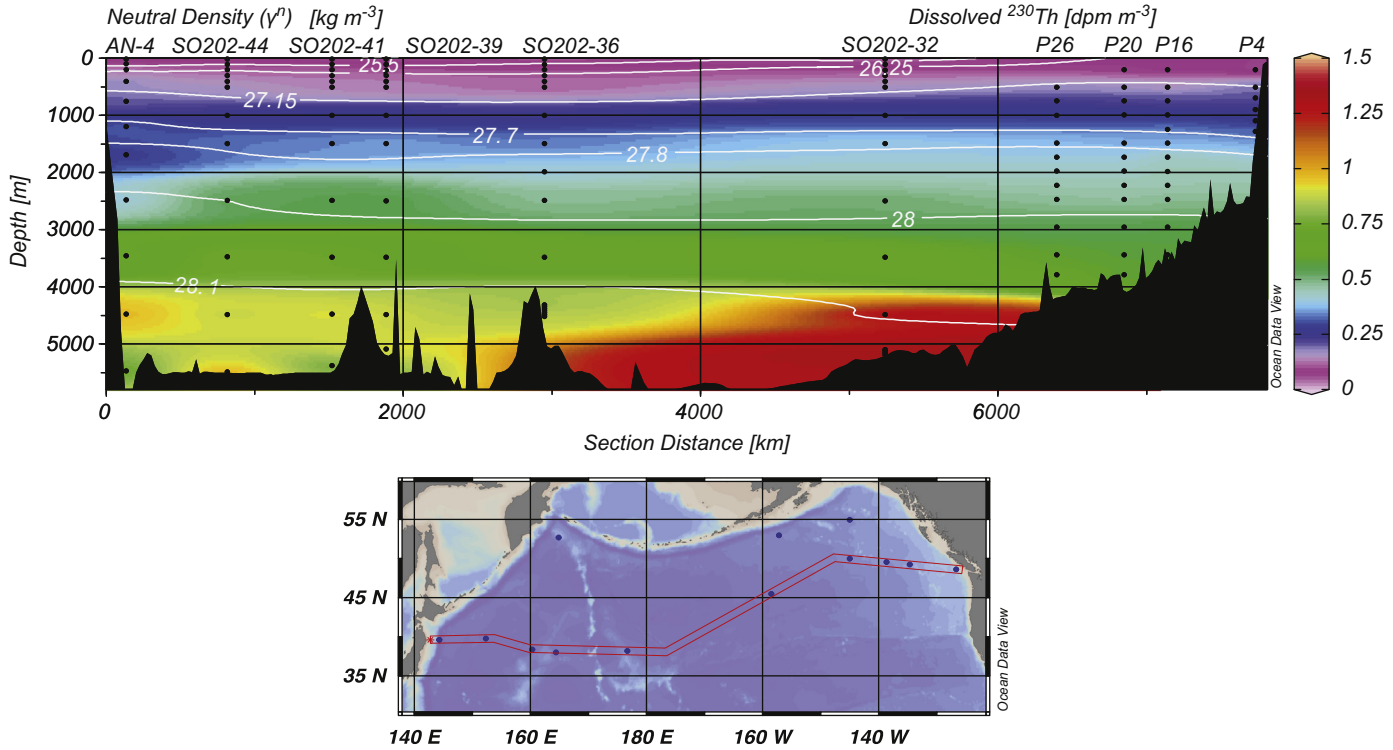

Fig. 4. North Pacific section of dissolved ^{230}Th (colormapping). White contours are isopycnals (neutral density). For comparison, none of the data in this figure have been corrected for detrital sources of ^{230}Th. Note that the high concentrations below 4500 m depth around 4000 km section distance are largely unconstrained by the data (shown as black dots).

advective contribution. Nonetheless, lateral mixing cannot explain the "missing" depletion of ^{230}Th at high scavenging intensity sites. Either our indicators of scavenging intensity or mixing rate are inadequate or ^{230}Th is displaying an unexpected insensitivity to variable scavenging intensities in the subarctic Pacific.

3.1.2. Subarctic North Pacific ^{230}Th anomalies

Station SO202-32 revealed much larger ^{230}Th concentrations (1.26–1.37 dpm m^{-3}) between 4484 m depth and the bottom (5301 m) than would be expected by extrapolating to greater depth the linear part of the profile (between 0 and 3.5 km depth). The neutral density horizon of this concentration anomaly (γ^n=28.10) also shows a positive concentration anomaly in dissolved Si in the area encompassing SO202-32 (~45–50°N and 150–170°W). Talley and Joyce (1992) linked this deep Si maximum to extreme age of the bottom water which allows a greater accumulation of dissolved Si from opal dissolution at the seafloor. Perhaps this water mass accumulates dissolved ^{230}Th due to its long isolation in a low-particle flux environment. Deep waters further south also have much higher ^{230}Th concentrations (Roy-Barman et al., 1996), but we consider the possibility of advective inflow of ^{230}Th unlikely as only weak, if any, northward currents propagate toward SO202-32 (Kawabe and Fujio, 2010).

The profiles from stations SO202-5, -24, -39, and -41 have negative deviations from linearity for the bottommost sample, taken within the benthic mixed layer, as defined by the well-mixed layer of potential temperature at the bottom of the CTD profile (Richards, 1990). Although we lack additional information about scavenging intensity in these benthic mixed layers, such as particle concentration, we suggest that the negative deviations in the [^{230}Th] profiles are the result of enhanced scavenging near the seafloor. Bottom scavenging of ^{230}Th has been found to influence many sites in the central North Pacific (Okubo et al., 2012). Sediments resuspended by deep currents, or more generally, by eddies and tidal mixing, could cause a scavenging environment with a larger K than the overlaying water column. We observe, however, that bottom scavenging does not always occur. At stations SO202-32, SO202-36, and the SAFe site (see below), 6–7 samples were taken equally spaced within 200 m of the seafloor and no significant vertical concentration gradients were observed. We infer from the spatial heterogeneity of bottom scavenging that local conditions, involving the interaction of eddies and tides with seafloor topography, influence the intensity of scavenging near the seabed.

The ^{230}Th depth profiles from Line P, SO202-5 and SO202-24 display some curvature (concave down) in the upper km. We interpret this not as reduced scavenging in upper waters but to be due to shoaling of the shallower isopycnals, associated with NPIW, from 45°N to 50°N (Macdonald et al., 2009). Isopycnal mixing probably supports some transfer of ^{230}Th from the south, where the isopycnal is deeper and [^{230}Th] higher, to shallower depths in the north, of course at a spatial scale concordant with the Th residence time. This situation is analogous to the ^{230}Th distributions in the Southern Ocean, where upward sloping isopycnals result in shoaling isolines of [^{230}Th] south of the polar front (Chase et al., 2003; Rutgers v. d. Loeff and Berger, 1993; Venchiarutti et al., 2011).

3.2. Response of ^{230}Th throughout the North Pacific and the nature of scavenging regimes

In contrast to the relatively homogeneous ^{230}Th profiles across the subarctic North Pacific, significant concentration gradients exist between our subarctic profiles and those reported for the subtropical gyre (Fig. 5a) (Anderson et al., 2012; François, 2007; Nozaki and Nakanishi, 1985; Nozaki and Yang, 1987; Okubo et al., 2012). Abyssal (> 4 km depth) waters reach [^{230}Th] of 2 dpm m^{-3} at SAFe and at several (sub)tropical sites reported by Okubo et al. (2012). While only considering the dissolved phase in our analysis, the observed subtropical–subarctic [^{230}Th] difference is larger (≥1 dpm m^{-3}) than can be accounted for by variable contributions of particulate matter (i.e. we expect a similar concentration difference in total ^{230}Th). Additionally, while the GEOTRACES intercalibration of seawater Th analyses revealed potential for inaccuracy between labs (Anderson et al., 2012), the subarctic–subtropical ^{230}Th contrast from INOPEX to SAFe (Fig. 5a) was produced by a single lab. The similar [^{230}Th] contrast between Line P and ALOHA is corroborative evidence against laboratory offsets here.

The contrast in abyssal ^{230}Th concentrations is relatively acute along the north–south transect between SO202-36 and BO-6, spanning the subtropics, nearly to the subarctic boundary (see Fig. 1). The lateral NPP and EP gradients between these stations are 66 and 34 mg C m^{-2} yr^{-1} km^{-1}, respectively, which are similar to or smaller than those found within the subarctic (Section 3.1.1). However, while the lateral [^{230}Th] gradient in the subarctic was small (d[^{230}Th]/dx < 1 × 10^{-4} dpm m^{-3} km^{-1}), between SO202-36 and BO-6, at 2.5 km, the lateral gradient is 2.3 × 10^{-4} dpm m^{-3} km^{-1}. The true lateral gradient may be larger than this, but it cannot be constrained without greater station density. There is no reason to expect smaller rates of lateral mixing in the north–south direction. Consequently, there must be a larger lateral gradient in scavenging intensity across the gyres than within the subarctic to explain the larger lateral concentration gradient in ^{230}Th.

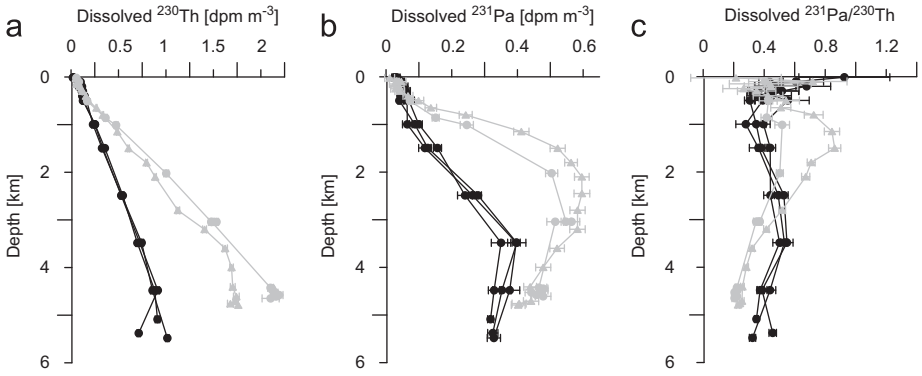

Fig. 5. Depth profiles of dissolved ^{230}Th (a), ^{231}Pa (b) and the ^{231}Pa/^{230}Th activity ratio (c) from SO202-39, -41, -44 in black compared with those from SAFe (gray circles) and ALOHA (gray triangles). Where error bars are not visible they are smaller than the symbol size. In (c), for clarity, ratios whose uncertainty is greater than ± 0.5 activity ratio units are not plotted.

To understand why ^{230}Th appears to respond to a scavenging gradient in one area (across gyres) and not another (within a gyre) we compare water column ^{230}Th inventories to a depth of 2.5 km for all locations in Fig. 1, except P4 where water depth is only 1323 m. At each included site, the seafloor is >800 m below 2.5 km, to avoid the influence of bottom scavenging. Also, at 2.5 km depth, neutral density does not vary greatly over the North Pacific ($\gamma^n = 27.98$–28.01). This inventory reflects a bulk average of scavenging intensity within the depth zone integrated.

Thorium-230 inventories from INOPEX, Line P, and AN-4 are within 25% of each other (Fig. 6a, Table 1). Yet NPP and EP range between 156–300 and 84–155 g C m^{-2} yr^{-1}, respectively (factors of 1.9 and 1.8). Two of the sites for which the dissolved inventory is estimated from total ^{230}Th in this NPP/EP range show relatively high inventories compared with the INOPEX and Line P locations. These sites (BO-1 and CY-5) are proximal to the INOPEX stations near 40°N, so it is unlikely that an advective influence is responsible for the discrepancy. The true value of K at BO-1 and CY-5 may be larger than 0.18 ± 0.09, the value assumed when converting total ^{230}Th to dissolved ^{230}Th (see Section 2.2). These sites would need, however, $K = 0.5$ to bring the inventories into better agreement. A value that high has typically only been found at very productive near-margin sites, for instance $K = 0.46$ in the Guatamala Basin (Bacon and Anderson, 1982) and $K = 0.52$ in the Japan Sea (Nozaki et al., 1987). Thus we cannot fully explain the high ^{230}Th inventories at BO-1 and CY-5.

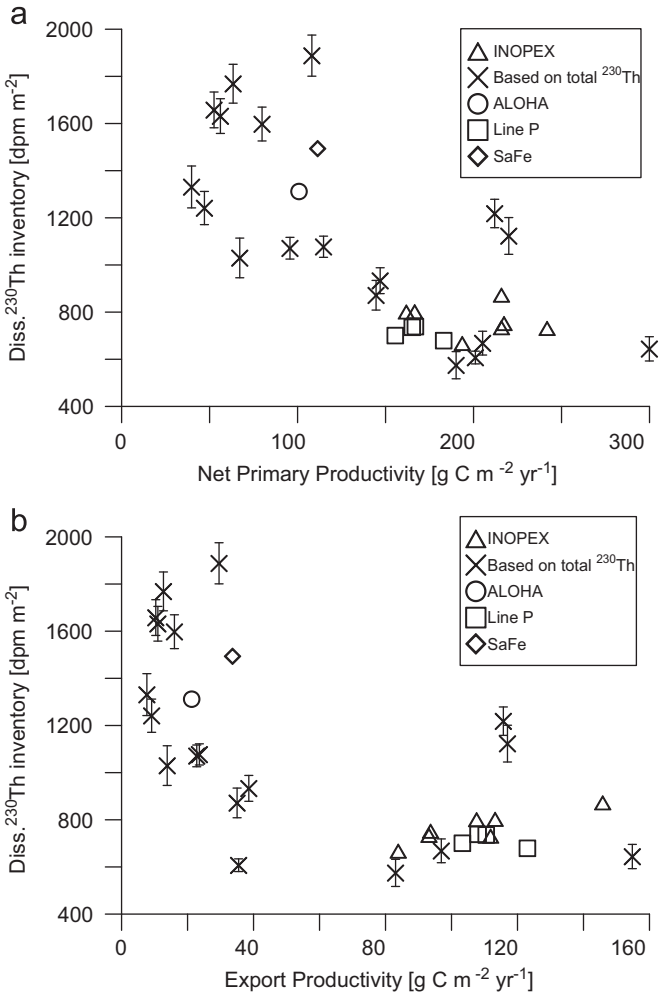

Fig. 6. Inventory of dissolved ^{230}Th from 0–2.5 km depth versus (a) Net Primary Productivity (NPP) and (b) Export Productivity (EP) for the INOPEX (triangles), Line P (squares), ALOHA (circles), and SAFE (diamond) stations and the sites for which total ^{230}Th data are available in the literature (*x*'s). Error bars on the points estimated from total ^{230}Th include the uncertainty in the distribution coefficient. Error bars based on dissolved data are roughly the size of the symbols and are omitted for clarity.

Thorium-230 inventories rise substantially as NPP and EP decline below 125 and 50 g C m^{-2} yr^{-1}, respectively (Fig. 6). Inventories at the two subtropical sites (ALOHA and SAFe) from which dissolved data are available rise to nearly twice the average of the subarctic sites. Dissolved inventories based on total ^{230}Th in the lower NPP/EP range are more variable but all are >1000 dpm m^{-2}. Variable contributions of detrital ^{230}Th or unaccounted variations in K across the (sub)tropical sites are unlikely to be large enough to explain this variability.

The observation that ^{230}Th inventories become much larger only below a certain NPP/EP level signifies an apparent threshold behavior for Th removal. Okubo et al. (2012) noted that [^{230}Th] roughly scaled inversely with bio-productivity among sites BO-4, HY-3, HY-2, and HY-1, as expected for a simple relationship between bioproductivity and scavenging intensity. Inclusion of sites from all across the North Pacific here, however, questions the robustness of such a simple relation. A step function of ^{230}Th inventory between high and low scavenging regimes may be more reflective of the data.

This step in Th inventories occurs across a specific threshold of NPP/EP, but the sites on either side of that threshold are geographically distinct. Sites with high and low ^{230}Th inventories largely coincide, respectively, with the subarctic and subtropical gyres, representing very different biomes (Longhurst, 1998). Large phytoplankton and diatoms are more prevalent in the subarctic while picoplankton dominate the subtropics (Alvain et al., 2008; Hashioka and Yamanaka, 2007). We hypothesize that disparate biogeographic communities produce particulate material with sufficiently contrasting physicochemical characteristics (such as surface area, chemical affinity of sorption sties, density, aggregation efficiency, etc.) to produce the threshold between scavenging regimes. This is not inconsistent with our present understanding of boundary scavenging but adds to our knowledge of its geographic scale. "Boundaries" may be more akin to particular biogeographic provinces rather than simply areas of enhanced particle flux. Future studies of marine particulate matter should seek to constrain which of the relevant particle characteristics vary most strongly across the Th scavenging regimes.

3.3. *Scavenging regimes for ^{231}Pa*

3.3.1. *INOPEX and (sub)tropical ^{231}Pa profiles*

The dissolved ^{231}Pa data from the INOPEX sites (Fig. 7), like those of ^{230}Th, are similar to each other when compared in depth profile. The upper (<2.5 km) and full water column residence times of dissolved ^{231}Pa at SO202-44 are 49 and 103 yr (vs. 11 and 22 yr for ^{230}Th), respectively. Isopycnal mixing for these timescales would cover a radius of ~1800 km in the upper water column, comparable to the SO202-36-44 transect, and 2550 km in the full water column, nearly encompassing the entire subarctic. Therefore within the subarctic, the concentration gradients imposed by variable scavenging intensity could be masked by the redistribution of ^{231}Pa by isopycnal mixing.

At station SO202-36, a sample at 996 m depth is outlying as anomalously high compared to the rest of the relatively smooth profile. The ^{230}Th and ^{232}Th analyses of this sample had no profile anomaly and the Pa mass spectrometry was repeated with the same result. We therefore attribute the anomalous ^{231}Pa data point to some other analytical error, perhaps sample-to-sample contamination after Pa had been separated from Th, and do not include it in our analysis.

Unlike the ^{230}Th results, the INOPEX ^{231}Pa profiles are in general non-linear, manifested primarily by a decrease or uniformity with

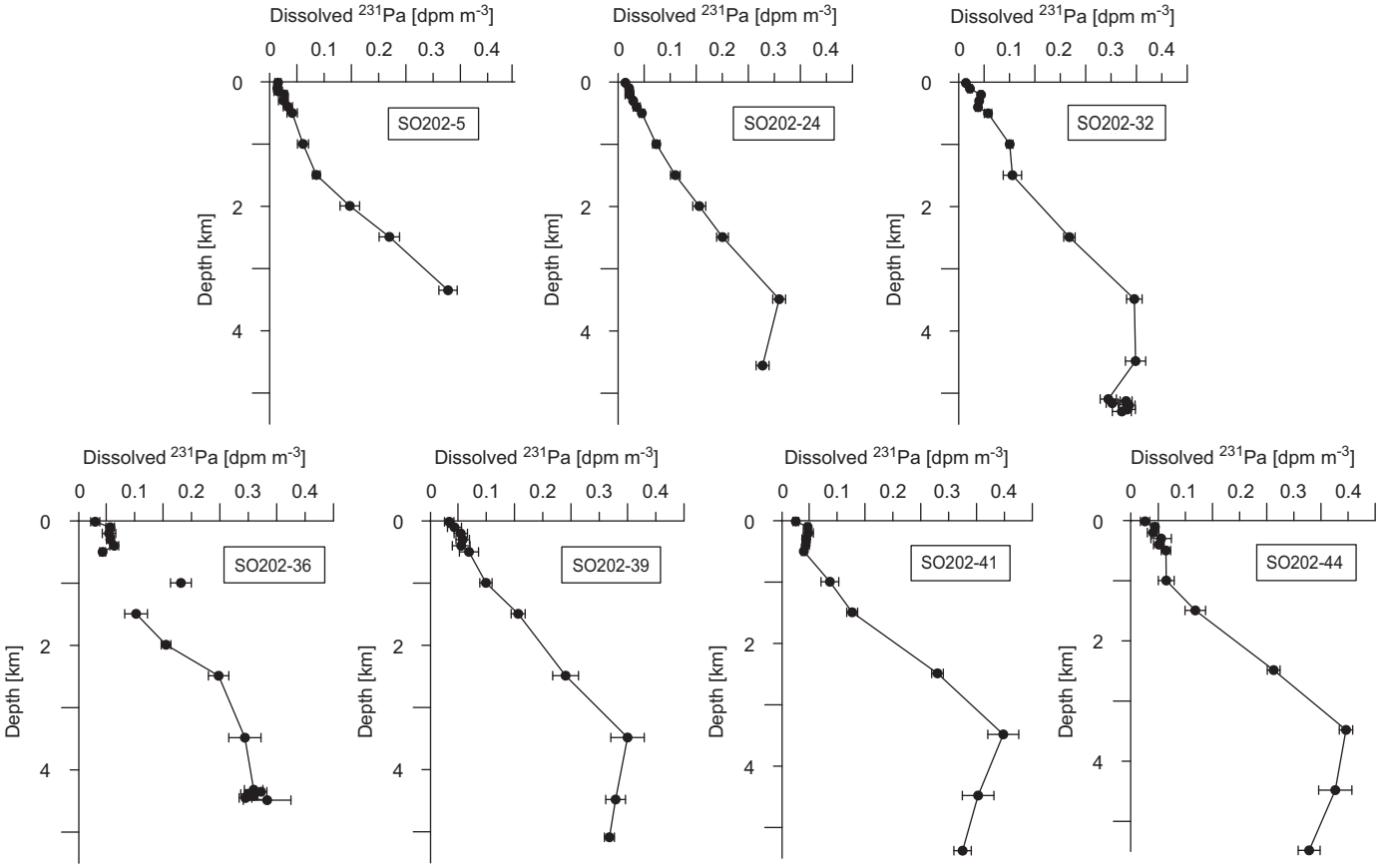

Fig. 7. Depth profiles of dissolved ^{231}Pa from the INOPEX locations (Fig. 1). These data have been corrected for the detrital ^{231}Pa based on measured dissolved ^{232}Th (see Section 2.2). The deepest sample in each profile is 5–15 m above the seafloor. Where error bars are not visible they are smaller than the symbol size.

depth of [^{231}Pa] at depths >3500 m (Fig. 7). Stations SO202-5 and SO202-36 do not fully resolve this feature, which the deeper INOPEX stations show consistently. Whatever factor is responsible for the anomalously high [^{230}Th] in the deepest samples of SO202-32 does not affect [^{231}Pa].

Concentrations of ^{231}Pa from the ALOHA and SAFe stations are generally larger than at the subarctic sites, at least between 1 and 3 km (Fig. 5b). Both subtropical profiles are non-linear, with [^{231}Pa] slightly decreasing at depths >2 km (compared with 3.5 km in the subarctic). Non-linear depth profiles of total ^{231}Pa have been reported (Nozaki and Nakanishi, 1985; Nozaki et al., 1998) for the (sub)tropical Pacific (CE-8, CE-13, and AN-1 in Fig. 1) which are generally in agreement with both ALOHA and SAFe.

3.3.2. *The upper water column (sub)tropical to subarctic contrast in ^{231}Pa*

Inventories down to 2.5 km (Fig. 8; Table 1) show a greater disparity between subarctic and subtropical sites (factor of 3) for ^{231}Pa than for ^{230}Th (factor of 2). In light of the five-fold greater residence time of dissolved Pa, which allows for more lateral homogenization by lateral mixing than for Th, this larger fractional difference in the upper water column inventory informs us that the difference in scavenging intensity between subarctic and subtropical regimes is far greater for Pa than for Th. This is actually captured in the modeling of dissolved ^{231}Pa in the North Pacific by Roy-Barman (2009), imposed by a larger relative difference in K from ocean margin to ocean interior for ^{231}Pa than for ^{230}Th. What is surprising from the INOPEX observations is that "the margin" appears not to be the thin zone of high productivity near the continents but the entire subarctic gyre. The (sub)tropical–subarctic contrast in the upper water column ^{231}Pa distribution also suggests a threshold type behavior related to the biological community contrast between the gyres.

The tendency of Pa to adsorb onto biogenic opal with greater affinity than other prevalent marine particulate phases (Chase et al., 2002; Geibert and Usbeck, 2004; Guo et al., 2002; Kretschmer et al., 2011; Scholten et al., 2005; Yu et al., 2001) is a natural way to link the chemical property of scavenging intensity to the biogeographic property of community structure. Opal concentration and flux is much larger in the subarctic than in the subtropical North Pacific (Bishop et al., 1999; Bishop and Wood, 2008; Karl et al., 2012; Lam et al., 2011; Scharek et al., 1999; Shibamoto and Harada, 2010). Greater fluxes of opal with high K values likely draw down [^{231}Pa] in the upper waters of the subarctic (Taguchi et al., 1989), so much so that a large lateral subtropical–subarctic concentration gradient is supported despite the influence of lateral mixing. Future paired measurements of particulate ^{231}Pa and opal in North Pacific GEOTRACES sections will test this hypothesis.

3.3.3. *Deepwater ^{231}Pa distributions and a proposed deep sink*

Negative deviations in [^{231}Pa] from linear profiles are observed in both the subarctic and subtropical regimes (Fig. 5b). The relative depletion of [^{231}Pa], as estimated by extending the linear profile in the upper 2 km downward and subtracting the observed profile, is larger for the subtropical sites than for the INOPEX sites. Whatever process is responsible for these depletions, the result is a relatively uniform distribution of [^{231}Pa] at great depth (3500–5500 m) across the North Pacific ([^{231}Pa] $=0.35$–0.5 dpm m^{-3}).

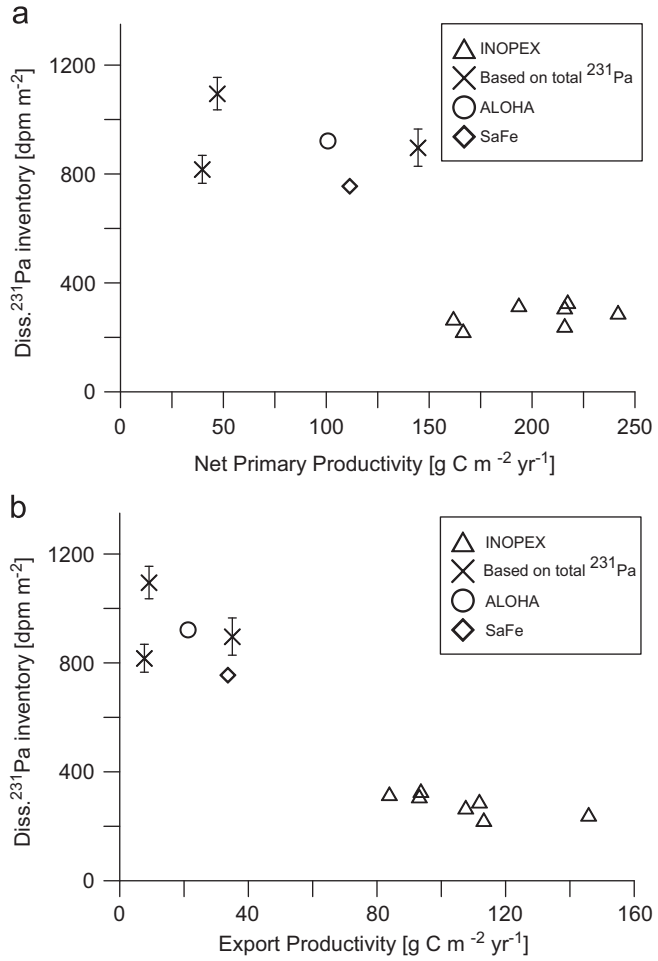

Fig. 8. Inventory of dissolved ^{231}Pa from 0–2.5 km depth versus (a) NPP and (b) EP for the INOPEX (triangles), Line P (squares), ALOHA (circles), and SAFE (diamond) stations and the sites for which total ^{231}Pa data are available in the literature (*x*'s). Error bars on the points estimated from total ^{231}Pa include the uncertainty in the distribution coefficient used in calculating the inventory. Error bars based on dissolved data are roughly the size of the symbols and are omitted for clarity.

Four possible explanations for deepwater depletions in North Pacific [^{231}Pa] can be suggested: (1) advective inflow of water with lower [^{231}Pa] from the south; (2) upwelling of LCDW into NPDW; (3) intense local scavenging by sediments at the seafloor and/or by resuspended sediments in nepheloid layers (McCave, 1986) (bottom scavenging); or (4) removal by lateral mixing to sites of higher scavenging intensity. We consider each explanation below.

The inflow of LCDW from the Southern Ocean to the subarctic along the western edge of the North Pacific could influence the INOPEX, ALOHA and SAFe profiles. Profiles of total ^{231}Pa from CE-8, CE-13 and AN-1 which are "upstream" of the INOPEX stations, however, show that [^{231}Pa] in LCDW is roughly 0.4–0.5 dpm m^{-3}, higher than or similar to that observed at the INOPEX stations. This is inconsistent with an advective input lowering deepwater [^{231}Pa] at the INOPEX sites. For the subtropical sites, advection is more difficult to discount because "upstream" ^{231}Pa data in the South Pacific are extremely limited. The one site with upstream water column ^{231}Pa data, M1 of the JGOFS-AESOPS program (53°S, 174.7°W), is situated at the beginning of the northward path of LCDW into the Pacific, and has [^{231}Pa] at this density horizon of similar magnitude to that seen in the (sub)tropics (~0.4 dpm m^{-3}) (Chase et al., 2003). However, given that the ageing of deep water between M1 and ALOHA is roughly 500 yr (Khatiwala et al., 2012; Matsumoto, 2007), one expects in-growth toward a linear profile to increase [^{231}Pa] along this route, as in North Atlantic Deep Water (Moran et al., 2002). Some other process, aside from lateral advection, must be removing ^{231}Pa from the deep North Pacific.

In terms of upwelling, explanation (2), and PMOC in general, the existing distribution of dissolved ^{231}Pa data is too sparse to evaluate the importance of this process. Another scavenged element with an ocean residence time in the order of or longer than that of Pa is Nd (Goldstein and Hemming, 2003). The isotopic composition of Nd (ε_{Nd}) does not show the non-radiogenic signature expected from southern-sourced water at BO-1, in the subarctic (Amakawa et al., 2009). Seawater profiles of ε_{Nd} from sites across the subtropical North Pacific (Amakawa et al., 2004, 2009; Piepgras and Jacobsen, 1988), including SAFe (Pahnke et al., 2012), indicate a characteristic presence of southern-sourced bottom water in the western but not the central or eastern subtropical Pacific. These observations argue against a basin-wide influence of bottom water inflow and subsequent upwelling on scavenged elements; however, because data on ε_{Nd} in the Pacific are also sparse, uncertainties exist as to whether it can be used to trace water masses as it is in the Atlantic (Jones et al., 2008).

Bottom scavenging, explanation (3), as the sole deep Pa-removal process, would require an unreasonably large vertical extension in the subtropics but it may be a factor for subarctic Pa. The full water column residence time of ^{231}Pa at SO202-44 and ALOHA is 103 and 173 yr, respectively. The resulting extent of vertical mixing influence in the subarctic is therefore 0.8–1.6 km, using Eq. (3) and $K_\rho = 1\text{–}4 \times 10^{-4}$ m^2 s^{-1}, which is comparable to the depth zone of subarctic ^{231}Pa depletion. The respective mixing scale at ALOHA is 1–2 km which is smaller than the subtropical depletion zone, 2.5–3 km above the bottom. Additionally, there is no measurable bottom depletion of ^{230}Th at the SAFe station, which would be expected if bottom scavenging of ^{231}Pa were occurring in the subtropics.

Removal by lateral mixing, explanation (4), is therefore the lead hypothesis for deep Pa depletions in the North Pacific, while bottom scavenging may be equally likely in the subarctic. Removal by lateral mixing implies some deep (> 2.5 km) ^{231}Pa sink somewhere in the Pacific, but our results do not reveal its location(s). Future studies, such as the GEOTRACES program, should seek to identify these deep Pa sinks as well as the processes involved. High scavenging intensity at the site of Pa removal could be manifested by a high vertical flux of particles in addition to a change in the chemical composition of particles. In particular, MnO_2, like biogenic opal, is known to have a strong affinity for Pa (Anderson et al., 1983). We hypothesize that authigenic Mn (oxy)hydroxide particles or coatings associated with reducing sediment conditions (Spencer et al., 1981) or hydrothermal vents and plumes (Anderson et al., 1990; Shimmield and Price, 1988) act as a predominant ^{231}Pa sink near continental margins and ridge crests, respectively.

In summary, Fig. 5c highlights the differences between subarctic and subtropical profiles of the dissolved ^{231}Pa/^{230}Th ratio. Uncertainties in the ratio are too large above 500 m to differentiate between the subarctic and subtropics. Within 0.5–2.5 km depth, however, the INOPEX profiles clearly have a lower ^{231}Pa/^{230}Th ratio, consistent with ^{231}Pa being more intensely scavenged in the subarctic because of greater opal abundance and with the conclusion that lateral mixing is not fast enough to overcome this imposed gradient. Below 2.5 km, the situation reverses, with lower ^{231}Pa/^{230}Th ratio in the subtropical profiles. This would be consistent with the classical concept of boundary scavenging, where a larger depletion of ^{230}Th (compared to that for ^{231}Pa) in the subarctic drives the increase in the ^{231}Pa/^{230}Th ratio. However, it appears the deep water ^{231}Pa/^{230}Th distribution is not strictly related to contrasting vertical particle flux but involves proximity to a deep ^{231}Pa sink to which ^{231}Pa is removed by lateral mixing to a greater extent in the subtropics.

4. Conclusions

Based on the available data, dissolved ^{230}Th and ^{231}Pa are uniformly distributed throughout the subarctic Pacific despite large spatial gradients in particle flux. Enhanced removal and corresponding depletion from the water column of ^{230}Th toward the margin, expected because of its short residence time, were absent in both the eastern and western subarctic regions. Large lateral [^{230}Th] gradients do exist between the subarctic and subtropical Pacific gyres and the relative contrast is even larger for [^{231}Pa] in the upper 2.5 km, despite its greater residence time. This indicates a much larger relative difference in scavenging intensity between the two regimes than within either regime, and the effect is greater for Pa than for Th. We suggest a threshold-like behavior between gyres in scavenging removal, tied to the distinct ecosystems that inhabit each gyre, with the larger response of ^{231}Pa linked to scavenging by opal in the subarctic. We conclude that the boundary scavenging concept applies to different spatial scales than originally proposed: gyre to gyre contrast rather than margin (or small zone of high scavenging intensity) to open ocean contrast, at least in the North Pacific.

In deepwater, the contrast in concentration between the subtropics and subarctic is smaller for ^{231}Pa than ^{230}Th, as expected from their respective residence times and the timescale for isopycnal mixing. We hypothesize that ^{231}Pa is strongly scavenged by a putative sedimentary Mn oxide sink primarily at depths >2.5 km throughout the North Pacific. The influence of PMOC on ^{231}Pa/^{230}Th distributions (Luo et al., 2012) cannot be ruled out quantitatively based on our data, although we have focused our interpretations primarily on the biogeographic nature of scavenging regimes.

Acknowledgments

We acknowledge the German Ministry of Education and Research (BmBF) for financially supporting the SO202-INOPEX cruise, the US National Science Foundation for funding the work at L-DEO (Award 1029211), and the Natural Sciences and Engineering Research Council of Canada and the Swiss National Science Foundation for the postdoctoral fellowship (Request no. PBEZ2-111588) that funded the work of SLJ at UBC. The R/V *Sonne* crew, all INOPEX participants, especially Jian Ren and Oliver Esper, are greatly acknowledged for help sampling on SO202. Discussions with Jerry McManus, Samar Khatiwala and Yiming Luo were helpful. We thank Walter Geibert, Mathieu Roy-Barman, and an anonymous reviewer for constructive reviews and the Editor, Gideon Henderson, for handling this manuscript. Figs. 1 and 4 were produced with Ocean Data View (R. Schlitzer, http://odv.awi.de, 2011). This is L-DEO Contribution 7678.

Appendix A. Supporting information

Supplementary data associated with this article can be found in the online version at http://dx.doi.org/10.1016/j.epsl.2013.03.008.

References

Alvain, S., Moulin, C., Dandonneau, Y., Loisel, H., 2008. Seasonal distribution and succession of dominant phytoplankton groups in the global ocean: a satellite view. Global Biogeochem. Cycles 22, GB3001.

Amakawa, H., Nozaki, Y., Alibo, D.S., Zhang, J., Fukugawa, K., Nagai, H., 2004. Neodymium isotopic variations in Northwest Pacific waters. Geochim. Cosmochim. Acta 68, 715–727.

Amakawa, H., Sasaki, K., Ebihara, M., 2009. Nd isotopic composition in the central North Pacific. Geochim. Cosmochim. Acta 73, 4705–4719.

Andersen, M.B., Stirling, C.H., Zimmermann, B., Halliday, A.N., 2010. Precise determination of the open ocean ^{234}U/^{238}U composition. Geochem. Geophys. Geosyst. 11, Q12003.

Anderson, R.F., Bacon, M.P., Brewer, P.G., 1983. Removal of ^{230}Th and ^{231}Pa at ocean margins. Earth Planet. Sci. Lett. 66, 73–90.

Anderson, R.F., Fleisher, M.Q., Robinson, L.F., Edwards, R.L., Hoff, J., Moran, S.B., Rutgers van der Loeff, M.M., Thomas, A.L., Roy-Barman, M., François, R., 2012. GEOTRACES intercalibration of ^{230}Th, ^{232}Th, ^{231}Pa, and prospects for ^{10}Be. Limnol. Oceanogr. Methods 10, 179–213.

Anderson, R.F., Lao, Y., Broecker, W.S., Trumbore, S.E., Hofmann, H.J., Wolfli, W., 1990. Boundary scavenging in the Pacific Ocean: a comparison of ^{10}Be and ^{231}Pa. Earth Planet. Sci. Lett. 96, 287–304.

Bacon, M.P., 1988. Tracers of chemical scavenging in the ocean: boundary effects and large-scale chemical fractionation. Philos. Trans. R. Soc. London, Ser. A 325, 147–160.

Bacon, M.P., Anderson, R.F., 1982. Distribution of thorium isotopes between dissolved and particulate forms in the deep sea. J. Geophys. Res. 87, 2045–2056.

Bacon, M.P., Spencer, D.W., Brewer, P.G., 1976. ^{210}Pb/^{226}Ra and ^{210}Po/^{210}Pb disequilibria in seawater and suspended particulate matter. Earth Planet. Sci. Lett. 32, 277–296.

Behrenfeld, M.J., Falkowski, P.G., 1997. Photosynthetic rates derived from satellite-based chlorophyll concentration. Limnol. Oceanogr. 42, 1–20.

Bishop, J.K.B., Calvert, S.E., Soon, M.Y.S., 1999. Spatial and temporal variability of POC in the northeast Subarctic Pacific. Deep Sea Res. Pt. II 46, 2699–2733.

Bishop, J.K.B., Wood, T.J., 2008. Particulate matter chemistry and dynamics in the twilight zone at VERTIGO, ALOHA and K2 sites. Deep Sea Res. Pt. I 55, 1684–1706.

Bown, J., Boye, M., Baker, A., Duvieilbourg, E., Lacan, F., Le Moigne, F., Planchon, F., Speich, S., Nelson, D.M., 2011. The biogeochemical cycle of dissolved cobalt in the Atlantic and the Southern Ocean south off the coast of South Africa. Mar. Chem. 126, 193–206.

Boyd, P.W., Ellwood, M.J., 2010. The biogeochemical cycle of iron in the ocean. Nat. Geosci. 3, 675–682.

Boyd, P.W., Trull, T.W., 2007. Understanding the export of biogenic particles in oceanic waters: is there consensus? Prog. Oceanogr. 72, 276–312.

Bradtmiller, L.I., Anderson, R.F., Sachs, J.P., Fleisher, M.Q., 2010. A deeper respired carbon pool in the glacial equatorial Pacific Ocean. Earth Planet. Sci. Lett. 299, 417–425.

Chase, Z., Anderson, R.F., Fleisher, M.Q., Kubik, P.W., 2002. The influence of particle composition and particle flux on scavenging of Th, Pa and Be in the ocean. Earth Planet. Sci. Lett. 204, 215–229.

Chase, Z., Anderson, R.F., Fleisher, M.Q., Kubik, P.W., 2003. Scavenging of ^{230}Th, ^{231}Pa and ^{10}Be in the Southern Ocean (SW Pacific sector): the importance of particle flux, particle composition and advection. Deep Sea Res. Pt. II 50, 739–768.

Chen, J.H., Lawrence Edwards, R., Wasserburg, G.J., 1986. ^{238}U, ^{234}U and ^{232}Th in seawater. Earth Planet. Sci. Lett. 80, 241–251.

Choi, M.S., Francois, R., Sims, K., Bacon, M.P., Brown-Leger, S., Fleer, A.P., Ball, L., Schneider, D., Pichat, S., 2001. Rapid determination of ^{230}Th and ^{231}Pa in seawater by desolvated micro-nebulization Inductively Coupled Plasma magnetic sector mass spectrometry. Mar. Chem. 76, 99–112.

Coale, K.H., Bruland, K.W., 1987. Oceanic stratified euphotic zone as elucidated by ^{234}Th:^{238}U disequilibria. Limnol. Oceanogr. 32, 189–200.

Delanghe, D., Bard, E., Hamelin, B., 2002. New TIMS constraints on the uranium-238 and uranium-234 in seawaters from the main ocean basins and the Mediterranean Sea. Mar. Chem. 80, 79–93.

Eppley, R.W., Peterson, B.J., 1979. Particulate organic matter flux and planktonic new production in the deep ocean. Nature 282, 677.

François, R., 2007. Paleoflux and paleocirculation from sediment ^{230}Th and ^{231}Pa/^{230}Th. In: Hillaire-Marcel, C., de Vernal, A. (Eds.), Developments in Marine Geology. Elsevier, pp. 681–716.

Geibert, W., Usbeck, R., 2004. Adsorption of thorium and protactinium onto different particle types: experimental findings. Geochim. Cosmochim. Acta 68, 1489–1501.

Gersonde, R., 2012. The expedition of the research vessel "Sonne" to the subpolar North Pacific and the Bering Sea in 2009 (SO202-INOPEX). Rep. Polar Mar. Res. 643, 323.

Goldberg, E.D., 1954. Marine geochemistry 1. chemical scavengers of the sea. J. Geol. 62, 249–265.

Goldstein, S.L., Hemming, S.R., 2003. Long-lived isotopic tracers in oceanography, paleoceanography, and ice-sheet dynamics. In: Elderfield, H., Holland, H.D., Turekian, K.K. (Eds.), Treatise on Geochemistry: The Oceans and Marine Geochemistry. Elsevier, pp. 453–489.

Guo, L., Chen, M., Gueguen, C., 2002. Control of Pa/Th ratio by particulate chemical composition in the ocean. Geophys. Res. Lett. 29, 1961.

Harrison, P., Whitney, F., Tsuda, A., Saito, H., Tadokoro, K., 2004. Nutrient and plankton dynamics in the NE and NW Gyres of the Subarctic Pacific Ocean. J. Oceanogr. 60, 93–117.

Hashioka, T., Yamanaka, Y., 2007. Seasonal and regional variations of phytoplankton groups by top–down and bottom–up controls obtained by a 3D ecosystem model. Ecol. Model 202, 68–80.

Holzer, M., Primeau, F.W., 2006. The diffusive ocean conveyor. Geophys. Res. Lett. 33, L14618.

Holzer, M., Primeau, F.W., 2008. The path-density distribution of oceanic surface-to-surface transport. J. Geophys. Res.: Oceans 113, C01018.

Honda, M.C., Watanabe, S., 2010. Importance of biogenic opal as ballast of particulate organic carbon (POC) transport and existence of mineral ballast-

associated and residual POC in the Western Pacific Subarctic Gyre. Geophys. Res. Lett. 37, L02605.
Honjo, S., Manganini, S.J., Krishfield, R.A., Francois, R., 2008. Particulate organic carbon fluxes to the ocean interior and factors controlling the biological pump: a synthesis of global sediment trap programs since 1983. Prog. Oceanogr. 76, 217–285.
Hsieh, Y.-T., Henderson, G.M., Thomas, A.L., 2011. Combining seawater ^{232}Th and ^{230}Th concentrations to determine dust fluxes to the surface ocean. Earth Planet. Sci. Lett. 312, 280–290.
Jones, K.M., Khatiwala, S.P., Goldstein, S.L., Hemming, S.R., van de Flierdt, T., 2008. Modeling the distribution of Nd isotopes in the oceans using an ocean general circulation model. Earth Planet. Sci. Lett. 272, 610–619.
Karl, D.M., Church, M.J., Dore, J.E., Letelier, R.M., Mahaffey, C., 2012. Predictable and efficient carbon sequestration in the North Pacific Ocean supported by symbiotic nitrogen fixation. Proc. Natl. Acad. Sci. USA 109 (6), 1842–1849.
Kawabe, M., 2008. Vertical and horizontal eddy diffusivities and oxygen dissipation rate in the subtropical Northwest Pacific. Deep Sea Res. Pt. I 55, 247–260.
Kawabe, M., Fujio, S., 2010. Pacific ocean circulation based on observation. J. Oceanogr. 66, 389–403.
Khatiwala, S., Primeau, F., Holzer, M., 2012. Ventilation of the deep ocean constrained with tracer observations and implications for radiocarbon estimates of ideal mean age. Earth Planet. Sci. Lett. 325–326, 116–125.
Kretschmer, S., Geibert, W., Rutgers van der Loeff, M.M., Schnabel, C., Xu, S., Mollenhauer, G., 2011. Fractionation of ^{230}Th, ^{231}Pa, and ^{10}Be induced by particle size and composition within an opal-rich sediment of the Atlantic Southern Ocean. Geochim. Cosmochim. Acta 75, 6971–6987.
Lam, P.J., Doney, S.C., Bishop, J.K.B., 2011. The dynamic ocean biological pump: Insights from a global compilation of particulate organic carbon, $CaCO_3$, and opal concentration profiles from the mesopelagic. Global Biogeochem. Cycles 25, GB3009.
Laws, E.A., Falkowski, P.G., Smith Jr., W.O., Ducklow, H., McCarthy, J.J., 2000. Temperature effects on export production in the open ocean. Global Biogeochem. Cycles 14, 1231–1246.
Locarnini, R.A., Mishonov, A.V., Antonov, J.I., Boyer, T.P., Garcia, H.E., Baranova, O.K., Zweng, M.M., Johnson, D.R., 2010. World Ocean Atlas 2009, Volume 1: Temperature. US Government Printing Office, Washington, DC.
Longhurst, A., 1998. Ecological Geography of the Sea. Academic Press, San Diego.
Luo, Y., Francois, R., Allen, S.E., 2010. Sediment ^{231}Pa/^{230}Th as a recorder of the rate of the Atlantic meridional overturning circulation: insights from a 2-D model. Ocean Sci. 6, 381–400.
Luo, Y., Francois, R., Allen, S.E., 2012. The influence of deep water circulation on the distribution of ^{231}Pa and ^{230}Th in the water column and sediments of the Pacific Ocean. Mineral. Mag. 75, 2042.
Macdonald, A.M., Mecking, S., Robbins, P.E., Toole, J.M., Johnson, G.C., Talley, L., Cook, M., Wijffels, S.E., 2009. The WOCE-era 3-D Pacific Ocean circulation and heat budget. Prog. Oceanogr. 82, 281–325.
Mahowald, N.M., Baker, A.R., Bergametti, G., Brooks, N., Duce, R.A., Jickells, T.D., Kubilay, N., Prospero, J.M., Tegen, I., 2005. Atmospheric global dust cycle and iron inputs to the ocean. Global Biogeochem. Cycles 19, GB4025.
Matsumoto, K., 2007. Radiocarbon-based circulation age of the world oceans. J. Geophys. Res. 112, C09004.
McCave, I.N., 1986. Local and global aspects of the bottom nepheloid layers in the world ocean. Neth. J. Sea Res. 20, 167–181.
Measures, C.I., Vink, S., 2000. On the use of dissolved aluminum in surface waters to estimate dust deposition to the ocean. Global Biogeochem. Cycles 14, 317–327.
Moran, S.B., Shen, C.C., Edmonds, H.N., Weinstein, S.E., Smith, J.N., Edwards, R.L., 2002. Dissolved and particulate ^{231}Pa and ^{230}Th in the Atlantic Ocean: constraints on intermediate/deep water age, boundary scavenging, and ^{231}Pa/^{230}Th fractionation. Earth Planet. Sci. Lett. 203, 999–1014.
Nozaki, Y., Horibe, Y., Tsubota, H., 1981. The water column distributions of thorium isotopes in the western North Pacific. Earth Planet. Sci. Lett. 54, 203–216.
Nozaki, Y., Nakanishi, T., 1985. ^{231}Pa and ^{230}Th profiles in the open ocean water column. Deep Sea Res. Pt. A 32, 1209–1220.
Nozaki, Y., Yamada, M., Nakanishi, T., Nagaya, Y., Nakamura, K., Shitashima, K., Tsubota, H., 1998. The distribution of radionuclides and some trace metals in the water columns of the Japan and Bonin trenches. Oceanol. Acta 21, 469–484.
Nozaki, Y., Yang, H.-S., 1987. Th and Pa isotopes in the waters of the western margin of the pacific near Japan: evidence for release of ^{228}Ra and ^{227}Ac from slope sediments. J. Oceanogr. 43, 217–227.
Nozaki, Y., Yang, H.-S., Yamada, M., 1987. Scavenging of thorium in the ocean. J. Geophys. Res. 92, 772–778.
Okubo, A., Obata, H., Gamo, T., Yamada, M., 2012. ^{230}Th and ^{232}Th distributions in mid-latitudes of the North Pacific Ocean: effect of bottom scavenging. Earth Planet. Sci. Lett. 339–340, 139–150.
Owens, W.B., Warren, B.A., 2001. Deep circulation in the northwest corner of the Pacific Ocean. Deep Sea Res. Pt. I 48, 959–993.
Pahnke, K., van de Flierdt, T., Jones, K.M., Lambelet, M., Hemming, S.R., Goldstein, S. L., 2012. GEOTRACES intercalibration of neodymium isotopes and rare earth element concentrations in seawater and suspended particles. Part 2: systematic tests and baseline profiles. Limnol. Oceanogr. Methods 10, 252–269.
Piepgras, D.J., Jacobsen, S.B., 1988. The isotopic composition of neodymium in the North Pacific. Geochim. Cosmochim. Acta 52, 1373–1381.
Richards, K.J., 1990. Physical processes in the benthic boundary layer. Philos. Trans. R. Soc. London, Ser. A 331, 3–13.
Robinson, L.F., Belshaw, N.S., Henderson, G.M., 2004. U and Th concentrations and isotope ratios in modern carbonates and waters from the Bahamas. Geochim. Cosmochim. Acta 68, 1777–1789.
Roy-Barman, M., 2009. Modelling the effect of boundary scavenging on thorium and protactinium profiles in the ocean. Biogeosciences 6, 3091–3197.
Roy-Barman, M., Chen, J.H., Wasserburg, G.J., 1996. ^{230}Th-^{232}Th systematics in the central Pacific Ocean: the sources and the fates of thorium. Earth Planet. Sci. Lett. 139, 351–363.
Roy-Barman, M., Lemaître, C., Ayrault, S., Jeandel, C., Souhaut, M., Miquel, J.C., 2009. The influence of particle composition on thorium scavenging in the Mediterranean Sea. Earth Planet. Sci. Lett. 286, 526–534.
Rutgers v. d. Loeff, M., Berger, G.W., 1993. Scavenging of ^{230}Th and ^{231}Pa near the antarctic polar front in the South Atlantic. Deep Sea Res. Pt. I 40, 339–357.
Rutgers v. d. Loeff, M., Geibert, W., 2008. U- and Th-series nuclides as tracers of particle dynamics, scavenging and biogeochemical cycles in the oceans. In: Krishnaswami, J.K., Cochran, J.K. (Eds.), Radioactivity in the Environment. Elsevier, pp. 227–268.
Scharek, R., Tupas, L.M., Karl, D.M., 1999. Diatom fluxes to the deep sea in the oligotrophic North Pacific gyre at Station ALOHA. Mar. Ecol. Prog. Ser. 182, 55–67.
Scholten, J.C., Fietzke, J., Mangini, A., Stoffers, P., Rixen, T., Gaye-Haake, B., Blanz, T., Ramaswamy, V., Sirocko, F., Schulz, H., Ittekkot, V., 2005. Radionuclide fluxes in the Arabian Sea: the role of particle composition. Earth Planet. Sci. Lett. 230, 319–337.
Shibamoto, Y., Harada, K., 2010. Silicon flux and distribution of biogenic silica in deep-sea sediments in the western North Pacific Ocean. Deep Sea Res. Pt. I 57, 163–174.
Shimmield, G.B., Price, N.B., 1988. The scavenging of U, ^{230}Th and ^{231}Pa during pulsed hydrothermal activity at 20 °S, East Pacific Rise. Geochim. Cosmochim. Acta 52, 669–677.
Spencer, D.W., Bacon, M.P., Brewer, P.G., 1981. Models of the distribution of ^{210}Pb in a section across the North Equatorial Atlantic Ocean. J. Mar. Res. 39, 119–138.
Taguchi, K., Harada, K., Tsunogai, S., 1989. Particulate removal of ^{230}Th and ^{231}Pa in the biologically productive northern North Pacific. Earth Planet. Sci. Lett. 93, 223–232.
Talley, L.D., Joyce, T.M., 1992. The double silica maximum in the North Pacific. J. Geophys. Res. 97, 5465–5480.
Taylor, S.R., McLennan, S.M., 1985. The Continental Crust: Its Composition and Evolution. Blackwell, Oxford.
Venchiarutti, C., Jeandel, C., Roy-Barman, M., 2008. Particle dynamics study in the wake of Kerguelen Island using thorium isotopes. Deep Sea Res. Pt. I 55, 1343–1363.
Venchiarutti, C., van der Loeff, M.R., Stimac, I., 2011. Scavenging of ^{231}Pa and thorium isotopes based on dissolved and size-fractionated particulate distributions at Drake Passage (ANTXXIV-3). Deep Sea Res. Pt. II 58, 2767–2784.
Weyer, S., Anbar, A.D., Gerdes, A., Gordon, G.W., Algeo, T.J., Boyle, E.A., 2008. Natural fractionation of ^{238}U/^{235}U. Geochim. Cosmochim. Acta 72, 345–359.
Yasuda, I., 2003. Hydrographic structure and variability in the Kuroshio–Oyashio Transition Area. J. Oceanogr 59, 389–402.
Yu, E.F., Francois, R., Bacon, M.P., Fleer, A.P., 2001. Fluxes of ^{230}Th and ^{231}Pa to the deep sea: implications for the interpretation of excess ^{230}Th and ^{231}Pa/^{230}Th profiles in sediments. Earth Planet. Sci. Lett. 191, 219–230.